

Short Timescale Coronal Variability in Capella

Vinay L. Kashyap¹, Jennifer Posson-Brown¹

ABSTRACT

We analyze 205 ks of imaging data of the active binary, Capella, obtained with the *Chandra* High Resolution Camera Imager (HRC-I) to determine whether Capella shows any variability at timescales < 50 ks. We find that a clear signal for variability is present for timescales $\lesssim 20$ ks, and that the light curves show evidence for excess fluctuation over that expected from a purely Poisson process. This overdispersion is consistent with variability at the 2-7% level, and suggests that the coronae on the binary components of Capella are composed of low-density plasma and low-lying loops.

Subject headings: stars: activity, stars: coronae, X-rays: stars

1. Introduction

Capella (α Aur; G1 III/G8 III) is the strongest non-solar coronal source accessible to high-sensitivity high-energy telescopes, and has been a common calibration target for X-ray and EUV instruments such as *EUVE*, *Chandra*, *XMM-Newton*, etc. It is a remarkably stable source, with no discernible flaring activity. Even though the emission structure has shown changes, especially in the high-temperature regime (see e.g., Dupree et al. 1996, Young et al. 2001), and there is considerable evidence for the dominant emission to change between the G1 III primary and the G8 III secondary (e.g., Linsky et al. 1998, Johnson et al. 2002, Ishibashi et al. 2006), the overall luminosity has remained steady over many years. For instance, Argiroffi et al. (2003) detected a change of 3% in *Chandra* HRC-S/LETGS data over the span of a year, and found no variability at timescales of 0.1 – 10 ks. Recently, analysis of *Chandra* ACIS-S/HETGS data (Raasen et al. 2007, Westbrook et al. 2007) found variations over long timescales, such as an $\approx 20\%$ intensity enhancement in early 2006, but no evidence for any variability at timescales $< 50 - 100$ ks.

Variability in stellar coronae is ubiquitous, and has been detected in all types of coronally active stars (Stassun et al. 2006, Caramazza et al. 2007, Westbrook et al. 2007, Güdel 2004,

¹Harvard-Smithsonian Center for Astrophysics, 60 Garden St., Cambridge, MA 02138

and references therein) and over a wide range of timescales (Kashyap & Drake 1999, Favata et al. 2005, Stassun et al. 2006, Pease et al. 2006, Colombo et al. 2007). This variability can occur due to many causes, ranging from cyclical dynamo variations (timescales of decades to years), to rotational modulation (months to hours), to active region evolution (hours to days), to flaring (hours to minutes). Generally, active stars are characterized by recurrent flares (see e.g., Güdel 2004) that are recognized in X-ray and EUV light curves as sudden increases in the luminosity followed by a slower decay. However, as activity increases, the flares start to occur closer in time to each other, and it becomes increasingly difficult to resolve them in the light curve (cf. Kashyap et al. 2001). Prominent flares are nevertheless detected in numerous active binaries (see e.g., Osten & Brown 1999, Osten et al. 2004).

Despite being one of the more coronally active stars, with a strong high temperature emission component (Brickhouse et al. 2000), flares have never been observed on Capella (Table 1). It is unknown whether this is due to a lack of flaring activity to contribute to the heating, or due to a preponderance of flares such that individual events cannot be distinguished (cf. Kashyap et al. 2001). Here we consider recent observations of Capella made with the *Chandra*/HRC-I (§2). We analyze these data and find that variability indeed can be detected at short timescales (§3), suggesting that the latter explanation is more plausible.

Table 1: Capella stellar properties

α Aur / GJ 194 / HD 34029 / HIP 24608 / HR 1708	
(R.A., Dec) $_{ICRS2000.0}$	(05:16:41.3591, +45:59:52.768)
distance	13.4 pc
orbital period	104 days
Components	G1 III / G8 III
Separation	109 R_{\odot}
Mass	2.56 / 2.69 [M_{\odot}]
Radius	9.2 / 12.2 [R_{\odot}]
M_V	0.14 / 0.25
$B - V$	0.74 / 0.87
rotational velocity	36 / 3 [km s^{-1}]

2. Data

Capella was observed as a calibration target with the *Chandra*/HRC-I over two cycles from December 2005 to January 2007 (see Figure 1). All the observations were carried out at



Fig. 1.— The combined light curve of all the *Chandra*/HRC-I observations of Capella, spanning 205 ks. The black histogram denotes the count rate for a binning of 100 s, and overlaid on it is the count rate for a binning of 500 s (green histogram). The data gaps between observations are excluded, and indicated by vertical red lines (solid when the gaps are > 100 s, dashed otherwise). The data comprise 40 ObsIDs (noted at the top of each segment, along with the day since 2005-dec-01 that the observation started). The SIM offset at which each observation is carried out is indicated at the bottom of each segment.

the telescope aimpoint, but at different locations on the detector corresponding to different offset values of the Science Instrument Module (SIM). The count rates shown in Figure 1 have been corrected for the QE (quantum efficiency) values at the observation location and thus represent flat-fielded light curves matched to the QE at the nominal aimpoint. The QE corrections are made separately for each bin of the light curves as the source dithers across the detector. Note however that this detailed correction is ignorable; it causes changes of $< 1\%$ when compared with count rates corrected with a QE averaged over the entire dither pattern (see also §3.3). We have reduced the data using the *Chandra* software for the interactive analysis of observations (CIAO v3.4) and using the most recent calibration products (CALDB v3.2). The high count rates observed ($\gtrsim 20$ ct s $^{-1}$), coupled with the sharp point spread function (PSF; it falls to 1% of the maximum at $\approx 1.3''$ away from the peak), provides an unprecedented opportunity to study small changes in the X-ray brightness of Capella. The source counts are extracted from a circle with radius 8x the size of the PSF ($\approx 10''$), and the background is locally estimated from a surrounding annulus of radii ($\approx 10\text{--}33''$). Assuming a Raymond-Smith thermal emission model with a dominant temperature component at 6 MK and a H column $N_H = 10^{18}$ cm $^{-2}$, we find with WebPIMMS¹ that the counts-to-energy conversion factor is $\sim 5.7 - 6.0 \times 10^{-12}$ ergs cm $^{-2}$ ct $^{-1}$ for different metallicities. This suggests X-ray luminosities of Capella in the 0.15–4.5 keV passband of $2.4 - 2.9 \times 10^{30}$ ergs s $^{-1}$ (cf. $L_X = 3.8 \times 10^{30}$ ergs s $^{-1}$ based on *Einstein*/IPC observations; Strassmeier et al. 1993).

3. Analysis and Discussion

3.1. Autocorrelation

It is clear from the HRC-I light curve (Figure 1) that Capella undergoes slow changes in its luminosity over timescales of weeks and months, with count rates ranging from $\approx 20 - 23$ ct s $^{-1}$. For instance, note the drop in intensity between ObsIDs 6552 and 6555, which are separated by 16 days,² and the difference between ObsIDs 6559 and 8360, which are done ≈ 1 yr apart, but are both carried out at the same detector location (thus precluding calibration differences as a factor; see §3.3 below).

This impression is confirmed by an autocorrelation analysis; we construct count rate

¹ <http://asc.harvard.edu/toolkit/pimms.jsp>

² The SIM offset also changes from -18 to -48 mm between these two observations, and it could be argued that uncalibrated differences in the QE uniformity may account for the drop in intensity. However, the similarity of count rates between observations 6558 and 6559, both of which were carried out on the same day, but at SIM offsets of -57 and 0 mm respectively, indicates that the drop in intensity is real.

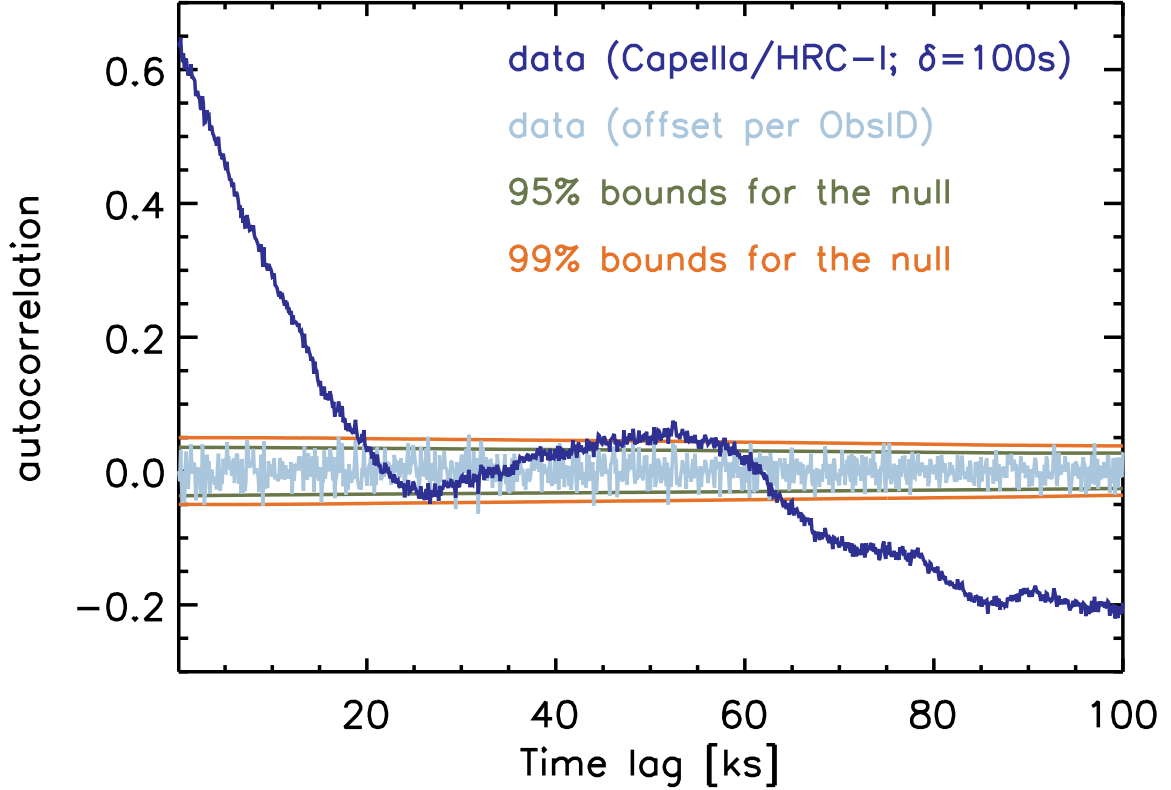


Fig. 2.— Autocorrelation in the light curve of Capella. The autocorrelation for a light curve binned by 100 s is shown as the dark blue curve, computed for different lag times. The expected autocorrelation for a light curve with no variability is 0 for all non-zero lag times, and the 95% and 99% uncertainty bounds on it are shown as horizontal lines (green and red respectively). The bounds are computed via Monte Carlo simulations of a flat light curve with the same mean and number of bins. There is clear evidence for variability at timescales $\lesssim 20$ ks. In contrast, the autocorrelation for a light curve constructed by offsetting it by the mean count rate in each ObsID (pale blue curve) shows no evidence of variability.

light curves $R(t_i; \delta)$ at various binning sizes δ and compute the autocorrelation

$$P(t_k; \delta) = \frac{\sum_{i=1}^{N_\delta - k} (R(t_i; \delta) - \nu(\delta))(R(t_{i+k}; \delta) - \nu(\delta))}{\sum_{i=1}^{N_\delta} (R(t_i; \delta) - \nu(\delta))^2},$$

where $\nu(\delta)$ is the average count rate in the N_δ bins in the light curve. The autocorrelation for $\delta = 100$ s is shown in Figure 2 as the dark blue curve (curves for other bin sizes are similar), along with estimates of the 95% and 99% uncertainties for each lag time t_k . These uncertainties are computed via Monte carlo simulations, by constructing 1000 light curves with the same number of bins as in $R(t_i; \delta)$, as Poisson deviates for an unvarying source intensity of $\nu(\delta) \cdot \delta$. The autocorrelation drops linearly until it becomes indistinguishable from statistical noise at a lag time of ≈ 20 ks; this is the typical signature of variability which occurs at timescales $\lesssim 20$ ks, such that count rates that are separated by longer timescales are essentially uncorrelated. At larger lag times, $\sim 30 - 60$ ks, the autocorrelation appears to rise again, but this is not distinguishable from statistical noise.³

This is consistent with the results found by Raasen et al. (2007) and Westbrook et al. (2007), who found similar variations over similar timescales. However, at a counts intensity level of ≈ 2 ct s⁻¹ (obtained from ACIS-S/HETG dispersed counts) they were unable to detect any variability at timescales $\lesssim 50$ ks corresponding to the durations of the observations, even using sophisticated algorithms such as the one described by Gregory & Loredó (1992). Here, we observe the source with a counts intensity an order of magnitude higher, and are thus able to investigate the variability at shorter timescales. Note that Argiroffi et al. (2003) also find no variability at timescales < 10 ks, but again, the HRC-S/LETGS data they rely on has count rates of $\lesssim 3$ ct s⁻¹, which is too small to detect the existence of variability on Capella.

Because the HRC-I observations are done in short segments, it is useful to consider the effect of removing large timescale effects on the autocorrelation. We thus reconstruct the light curve by offsetting that computed in each ObsID by the average intensity of the source during that ObsID (i.e., for each segment the average count rate is set to 0), and recompute the autocorrelation. This has the effect of completely removing variations at timescales greater than $\approx \frac{1}{2}$ of the typical exposure time, and will reveal any variability that may exist

³ At even larger lag times, $t_k > 65$ ks, the autocorrelation drops further and becomes significantly < 0 , suggesting that the count rates are anticorrelated at large timescales, i.e., the intensity tends to fluctuate over long temporal separations. However, these values are not physically meaningful, since the data gaps between observations are large and the lag time ceases to be a useful construct. Note that typical observation times are 5 ks, and the observation times for contiguous ObsIDs ranges from 12 to 62 ks, with a median of 19 ks (see Figure 1).

at very small timescales. The result of this is shown as the pale blue curve in Figure 2. This is everywhere consistent with no variability. Because the typical observation time is 5 ks, this suggests that there is no variability on Capella at timescales $\lesssim 3$ ks. Note that offsetting the light curves by different amounts at different times, as we have done in this exercise, introduces additional statistical uncertainty into the results because of a non-stationary bias, and therefore the power of the test to detect a variability signal is decreased. In order to determine whether there does exist variability over timescales of ~ 5 ks, we test the dispersion of the fluctuations (see §3.2).

3.2. Overdispersion

The large count rates of Capella seen with the HRC-I afford us the capability to analyze the light curve at short timescales. In order to test the constancy of the intensity within each ObsID, we carry out a Kolmogorov-Smirnov (K-S) test on the photon arrival time data in each ObsID. A large fraction of the datasets show evidence that the null hypothesis of no variation within an observation can be rejected: 17% have $p < 0.05$, and 37% have $p < 0.1$. This is not strong evidence for short timescale variability, but the repeated rejection of the null at a frequency larger than expected indicates the possible existence of intermittent variability. Also note that the K-S test generally has low power in detecting small, slow variations, and a better test is required. For that, we consider whether the observed fluctuations in the light curve are consistent with statistical deviations. Such a test is also of value in establishing the magnitude of the residual calibration errors (see §3.3).

The HRC-I light curve (Figure 1) shows numerous sharp fluctuations similar to that expected from Poisson fluctuations. We have tested whether these fluctuations are consistent with such a picture, and conclude that they are not; the observed fluctuations are invariably *overdispersed* compared to the expected Poisson deviations (see Figure 3). In particular, given a counts light curve $C(t_i; J, \delta)$ for ObsID J , where t_i are the N_δ time bins resulting from choosing a bin of size δ , we summarize the light curve with its mean $\mu_J(\delta)$ and variance $\sigma_J^2(\delta)$ and compute three measures of overdispersion:

$$\rho_{\text{frac}} \equiv \frac{\sigma_J(\delta)}{\sqrt{\mu_J(\delta)}}, \quad (1a)$$

$$\rho_{\text{diff}} \equiv \frac{\sigma_J^2(\delta) - \mu_J(\delta)}{\mu_J(\delta)}, \quad (1b)$$

$$\rho_{\chi^2} \equiv \sum_{i=1}^{N_\delta} \frac{[C(t_i; J, \delta)^2 - \mu_J(\delta)]^2}{N_\delta \mu_J(\delta)}. \quad (1c)$$

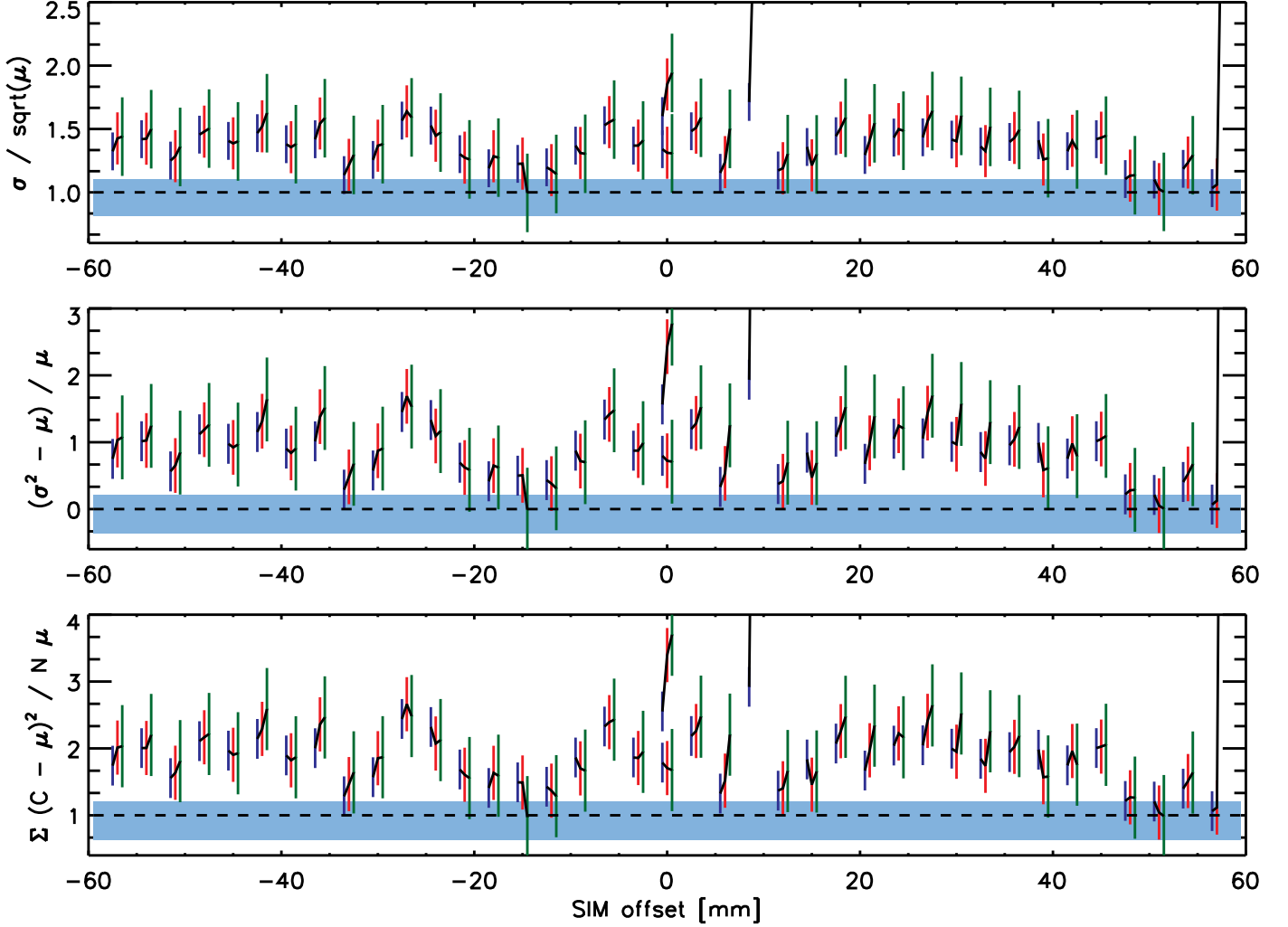


Fig. 3.— Overdispersion in the light curve in each Capella ObsID. The overdispersion measures ρ_{frac} (top), ρ_{diff} (middle), and ρ_{χ^2} (bottom) are calculated for each ObsID for different values of the light curve bin sizes $\delta = 25, 50, 100$ s, and are denoted by the thin vertical lines grouped around the SIM offset for that observation. The lines are offset from each other for clarity and have δ increasing from left to right, and the measured values for each ObsID are connected by dark lines. The vertical lines represent the $\pm 3\sigma$ error bars for the *null*, determined from Monte Carlo simulations of a model without any intrinsic variability but matching the count rate and exposure time of the observation. The values expected for the null model are shown for each $\rho_{(\cdot)}$ as the horizontal dashed line. The overdispersion measures computed for the combined HZ 43 data (for a binning that matches $\delta = 25$ s for Capella) is shown as the pale blue band whose width corresponds to the $\pm 3\sigma$ error bounds determined the same way as for Capella.

If the light curve fluctuations are fully explained as Poisson fluctuations, we must have $\rho_{\text{frac}} \approx 1$, $\rho_{\text{diff}} \approx 0$, and $\rho_{\chi^2} \approx 1$, since the variance of a Poisson process is equal to its mean.⁴ In contrast, if an additional process is operating to cause variations in the source intensity, we must have $\rho_{\text{frac}} > 1$, $\rho_{\text{diff}} > 0$, and $\rho_{\chi^2} > 1$.

Table 2: Average overdispersion

δ [s]	ρ_{frac}	ρ_{diff}	ρ_{χ^2}
25	1.35±0.15	0.84±0.40	1.83±0.40
50	1.41±0.31	1.08±1.26	2.06±1.25
100	1.50±0.43	1.44±1.87	2.39±1.84

For the HRC-I dataset, computing the overdispersion measures for all ObsIDs, for a variety of time binning sizes ($\delta = 25, 50, 100$ s), we find that the latter condition holds (Figure 3; see also Table 2) for the majority of the cases. In each case, we compute the error bars on $\rho_{(\cdot)}$ via Monte Carlo simulations of the null model, and thereby determine the significance of each measurement of the overdispersion measure by calibrating the statistic independently for the specific values of $\{\mu, N_\delta\}$. Thus, we find that in most of the observations, the overdispersion is significant, and hence that the observed variations in the Capella light curves cannot be explained as due only to Poisson fluctuations. In particular, we find $\rho_{\text{frac}} \approx 1.37 - 1.45$, $\rho_{\text{diff}} \approx 0.87 - 1.09$, and $\rho_{\chi^2} \approx 1.86 - 2.05$ as the range of the medians over the entire dataset for the three different bin sizes considered. The overdispersions tend to increase with δ , as is expected because the relative statistical error decreases with increasing counts. The averages and the standard deviations are reported in Table 2 for each δ , and show that the result is robust over different methods and binning sizes. The measured points are in every case except one greater than the nominal value for the null, and the large standard deviations arise from large deviations upward. Thus we conclude that Capella exhibits variability over durations that characterize the observations, i.e., at timescales ~ 5 ks. More sophisticated analyses (which are in progress) are necessary to fully characterize this variability.

These measurements suggest that the intrinsic variability has an effect that is of similar magnitude to the Poisson process, and that we are able to detect it primarily because of the large count rates and because the large number of independent datasets allows us to check that all give similar results. Our analysis does not allow a direct calculation of the

⁴ Note that unlike the autocorrelation analysis above, here we use counts light curves in order to maintain the correspondence with a Poisson statistical process; the effect of QE non-uniformity is negligible, as described in §2, and as demonstrated explicitly in §3.3.

intensity variations that result in these overdispersion values, but assuming a model with small deviations, we estimate that intensity variations of the order $\frac{\Delta C}{C} \approx 0.02 - 0.07$ are consistent with the observed $\rho_{(.)}$. Since such intensity variations are of the same order as the expected Poisson fluctuations in the light curves, it is not surprising that methods such as the Kolmogorov-Smirnoff test and Fourier analysis fail to detect the existence of the subtle variability in the data. Similarly, Argiroffi et al. (2003) place a 3σ limit on the variability at $< 5 - 10\%$, based on *Chandra* HRC-S/LETGS data where Capella has a count rate of $\approx 2.7 \text{ ct s}^{-1}$. With the HRC-I, count rates ≈ 8 times higher are observed, which allows us to detect the existence of such variability at $> 3\sigma$ (Figure 3).

3.3. Calibration

As the source position changes on the detector with each observation, and even during a single observation as it dithers across the detector, the source passes over regions with different quantum efficiencies (QE). Variations in the QE will lead to corresponding differences in the observed count rate, and may produce a false signal of variability. In comparing the source intensities from different ObsIDs, we have taken the QE variations into account using the current best estimate of the HRC-I QE map, which is estimated to be accurate to $\approx 5\%$ across the detector (Posson-Brown & Donnelly 2004; Figure 1 suggests that the relative error in the QE map is considerably lower). While computing the overdispersion measures however, we do not make such corrections in order to not bias the statistical estimates. Instead, we estimate the contribution of the local variations in QE to the overdispersion by comparing the variances in the light curves generated with and without correcting for this effect: the observed $\sigma(\delta)$ increases by $\lesssim 3\%$, which is negligible compared to the magnitude of the observed overdispersions (Figure 3). As a further test, we have carried out Fourier transforms of the counts light curves; these show no evidence of a periodic signal, as would be present at frequencies corresponding to the dither periods if QE variations were to make a significant contribution to the variability. In addition, we place a direct limit on the residual calibration uncertainty by comparing the analysis of Capella with that of a known non-varying source, HZ 43.

HZ 43 is a H-rich DA white dwarf with a temperature $T_{\text{eff}} \approx 50 \text{ kK}$ (Dupuis et al. 1998). It has no known or expected variability, and thus serves as a comparison target to verify the effect of the residual calibration uncertainty. The source has been observed numerous times as a calibration target by *Chandra* in the HRC-I+LETGS configuration, and has thus far been observed for a total of 31.3 ks at the nominal aimpoint. The observed count rate is 3.6 ct s^{-1} , and coincidentally the accumulated counts approximately matches

the number of counts produced in any given Capella ObsID, making it an excellent proxy to test for the existence of any instrument-based variability.⁵ We measure the overdispersion in HZ 43 at various bin sizes, set such that the same number of counts are expected in each bin as for the Capella data. For instance the Capella light curve binned at $\delta = 25$ s is approximately matched by a HZ 43 light curve binned at $\delta = 140$ s; i.e., absent intrinsic variations, and assuming that the magnitude of the local QE variations are spatial scale independent, both curves should have identical statistical properties. We find that the HZ 43 overdispersion measures are fully consistent with there being no intrinsic variability whatsoever (see Figure 3), and thus serve to confirm the detection of overdispersion in the Capella data.

3.4. Coronal Structure

Stellar coronae are generally considered to be analogous to the solar corona, in the sense that the X-ray emission arises from optically thin, collisionally excited plasma, which is organized in active regions by magnetic fields and is probably heated by magnetic reconnection events. In the case of Capella, the energetics indeed support this view: the surface area of both components is ≈ 100 times that of the Sun (Table 1), and the X-ray luminosity is correspondingly higher, at ≈ 100 times the solar luminosity at the peak of its activity cycle. This is consistent with the picture of a solar like atmosphere, with the coronae dominated by loops in active regions that cover a large fraction of the surface. However, the temperatures on Capella’s coronae are significantly hotter, and the strong emission component at $T \sim 6$ MK has no corresponding structure on the Sun.

We have established above (§§3.1,3.2) that Capella exhibits variability over timescales ranging from $\tau \sim 5 - 20$ ks. While the longer timescale variability could arise simply due to slow evolution of active regions, the variability at shorter timescales ($\gtrsim 5$ ks) is likely due to the dynamical balance of heating events and cooling. Because Capella maintains its luminosity to within a few percent, it must be that heating and cooling events are in balance for the most part, and therefore the variability timescale must be matched to the total coronal heating rate changes, and hence to the radiative cooling timescales. (For typical coronal densities, conductive cooling is not a factor at these timescales.) We can estimate the physical characteristics of the Capella coronae based on this correspondence. The cooling

⁵ HZ 43 has also been observed at other times and other locations on the HRC-I, but these observations do not have sufficient counts for a useful comparison with Capella data. Furthermore, the off-axis pointings also have large PSFs, which again precludes direct comparisons.

timescale,

$$\tau = \frac{k_B T}{n_e \Lambda(T)}, \quad (2)$$

where n_e is the electron number density, and $\Lambda(T)$ is the power emitted by a unit volume of the plasma at temperature T . Adopting a coronal temperature of $\log T = 6.8$, and a metallicity $Z = 0.6$ (see Brickhouse et al. 2000), the power emitted is $\Lambda \approx 2.3 \times 10^{-23}$ ergs $\text{cm}^3 \text{s}^{-1}$, and we estimate the coronal number density

$$n_e = 4 \times 10^9 \tau_{10}^{-1} \text{ cm}^{-3}, \quad (3)$$

where $\tau_{10} = \frac{\tau}{(10 \text{ ks})}$. This is consistent with the limit $n_e \lesssim 10^{10.2} \text{ cm}^{-3}$ found by Ness et al. (2003) based on an analysis of the Ne IX triplet in *Chandra* and XMM-Newton grating data. For the observed luminosity (see §2) and the adopted temperature, the volume emission measure $EM \approx 10^{53} \text{ cm}^{-3}$. Assuming that the emission is spread uniformly across the surface of both stars, and adopting a visible surface area 100 times that of the Sun, we estimate the height of the corona

$$h_{\text{est}} \approx 1.3 \times 10^9 \tau_{10}^2 f_{\text{fill}}^{-1} \text{ cm}, \quad (4)$$

where f_{fill} is the surface filling fraction of active regions. This is comparable to the typical loop sizes seen on the Sun, but is small compared to the density scale height on Capella, $h_{\text{scale}} \approx 8 \times 10^{11} \text{ cm}$.

We assume here that the entire corona is part of the balance between the heating and cooling occurring at the detected variability timescales. It is possible however that there are multiple components of emission in the corona: the small timescale variability may be due to a small portion of the corona, e.g., as in X-ray bright points on the Sun, and the bulk of the emission may arise in a lower density component that cools slowly and is heated correspondingly slower and reaches to a height comparable to the density scale height. However, this scenario appears to be ruled out by the analysis of high-resolution EUV spectra by Sanz-Forcada, Brickhouse, & Dupree (2003), who suggest that the bulk of the plasma on Capella is at high densities. Note that while we have confined our attention to $\tau = 5 - 20 \text{ ks}$, we cannot formally rule out variability at shorter timescales (more sophisticated analyses are in progress). Such variability will act to increase the estimate for the coronal density n_e and decrease the height of the emission layer h_{est} . We speculate that the most probable scenario for emission on Capella is one where it is dominated by numerous low-lying activity sites.

4. Summary

We have analyzed a deep *Chandra*/HRC-I observation of the active binary Capella to detect variability at timescales shorter than 50 ks. Capella is a highly stable coronal source on which hitherto no short term variability had been seen, despite its relatively high activity level. The HRC-I is uniquely positioned to achieve this objective because it allows the measurement of large count rates ($\gtrsim 20$ ct s $^{-1}$) with no pileup effects. The unprecedented data quality allows us to test for the existence of variability at timescales as short as 5 ks.

We confirm the conclusion of Argiroffi et al. (2003), Raasen et al. (2007), and Westbrook et al. (2007) that Capella exhibits intensity variations at the 3 – 10% level over timescales of months and years, but unlike those studies which were limited in statistical power due to low count rates, we detect variability at timescales < 50 ks.

We apply numerous statistical tests such as autocorrelation, overdispersion, K-S, etc., to the data, both cumulatively and in individual observation segments, and find that variability does exist at timescales $\tau = 5 - 20$ ks. This suggests that the coronal plasma is at a relatively low density ($n_e \lesssim 10^9$ cm $^{-3}$) and that the emission arises in low-lying loops with heights $\sim 10^9$ cm.

This work was supported by the Chandra X-ray Center NASA contract NAS8-39073. We thank Brad Wargelin, Frank Primini, Jeremy Drake, Mike Juda, Nancy Evans, and Scott Wolk for useful discussions.

REFERENCES

- Argiroffi, C., Maggio, A., & Peres, G., 2003, *A&A*, 404, 1033
- Brickhouse, N.S., Dupree, A.K., Edgar, R.J., Liedahl, D.A., Drake, S.A., White, N.E., Singh, K.P., 2000, *ApJ*, 530, 387
- Caramazza, M., Flaccomio, E., Micela, G., Reale, F., Wolk, S.J., & Feigelson, E.D., 2007, *A&A*, 471, 645
- Colombo, J.F.A., Caramazza, M., Flaccomio, E., Micela, G., & Sciortino, S., 2007, *astro-ph/0708.2399*
- Dupree, A.K., & Brickhouse, N.S., 1996, in *Poster Proc., IAU Symp. 176: Stellar Surface Structure* (Wien: Institut für Astronomie), 184
- Dupuis, J., Vennes, S., Chayer, P., Hurwitz, M., Bowyer, S., 1998, *ApJL*, 500, L45
- Favata, F., Flaccomio, E., Reale, F., Micela, G., Sciortino, S., Shang, H., Stassun, K.G., & Feigelson, E.D., 2005, *ApJS*, 160, 469F
- Güdel, M., 2004, *A&ARev*, 12, 71
- Ishibashi, K., Dewey, D., Huenemoerder, D. P., & Testa, P., 2006, *ApJ*, 644, 117
- Johnson, O., Drake, J. J., Kashyap, V., Brickhouse, N. S., Dupree, A. K., Freeman, P., Young, P. R., & Kriss, G.A., 2002, *ApJ*, 565, 97
- Kashyap, V., & Drake, J.J., 1999, *ApJ*, 524, 988
- Kashyap, V.L., Drake, J.J., Güdel, M., & Audard, M., 2002, *ApJ*, 580, 1118
- Linsky, J. L., Wood, B. E., Brown, A., & Osten, R. A., 1998, *ApJ*, 492, 767
- Ness, J.-U., Brickhouse, N.S., Drake, J.J., & Huenemoerder, D.P., 2003, *ApJ*, 598, 1277
- Osten, R.A., Brown, A., Ayres, T.A., Drake, S.A., Franciosini, E., Pallavicini, R., Tagliaferri, G., Stewart, R.T., Skinner, S.L., & Linsky, J.L., 2004, *ApJS*, 153, 317
- Osten, R.A., & Brown, A., 1999, *ApJ*, 515, 746
- Pease, D.O., Kashyap, V.L., Ratzlaff, P.W., Drake, J.J., Evans, N.R., Mossman, A.E., Kim, D., Green, P.J., & the ChaMP Collaboration, 2006, *AAS-HEAD*, 9, 01.01
- Posson-Brown, J., & Donnelly, R.H., 2004, at the *Chandra* Calibration Workshop, 25 Oct 2004
- Raassen, A. J. J., Kaastra, J. S., *A&Ap*, 461, 679
- Sanz-Forcada, J., Brickhouse, N.S., & Dupree, A.K., 2003, *ApJS*, 145, 147
- Stassun, K.G., van den Berg, M., Feigelson, E., & Flaccomio, E., 2006, *ApJ*, 649, 914

- Strassmeier, K.G., Hall, D.S., Fekel, F.C., & Scheck, M., 1993, A&AS, 100, 173
- Westbrook, O.W., Evans, N.R., Wolk, S.J., Kashyap, V.L., Nichols, J.S., Mendygral, P.J., Slavin, J.D., & Waldron, W.L., 2007, ApJS, submitted
- Young, P. R., Dupree, A. K., Wood, B. E., Redfield, S., Linsky, J. L., Ake, T. B., & Moos, H. W., 2001, ApJ, 555, L121